Winterer, E.L., Sager, W.W., Firth, J.V., and Sinton, J.M. (Eds.), 1995
Proceedings of the Ocean Drilling Program, Scientific Results, Vol. 143

9. SMALL-SCALE SHALLOW-WATER CARBONATE SEQUENCES OF RESOLUTION GUYOT (SITES 866, 867, AND 868)[1]

André Strasser,[2] Hubert Arnaud,[3] François Baudin,[4] and Ursula Röhl[5]

ABSTRACT

The Hauterivian to upper Albian carbonate sediments drilled on Resolution Guyot are all of shallow-water origin. The volcanic basement is covered by dolomitized oolitic and oncolitic grainstones of an inner-ramp setting. At 1400 m below seafloor (mbsf), they pass into peritidal facies punctuated by small coral and rudist bioherms and by beach sediments. Oolites dominate between 790 and 680 mbsf. The upper part of the guyot (from 680 mbsf up to the phosphate-iron-manganese crust capping the Cretaceous platform) is composed of lagoonal carbonates exhibiting some calcrete horizons. The material collected from Holes 867B and 868A implies that the platform was rimmed by barrier islands and storm beaches, and that reefs (rudists and sponges) were of minor importance. This is in contrast to modern atolls, where reefs are the major rim builders. In the late Albian, the platform was subaerially exposed and karstified, then drowned.

Although average recovery was low (15.4% for Hole 866A, 29.2% for 867B, 46.3% for 868A), the cored material clearly shows that the sedimentary record is composed of small, meter-scale sequences. They are especially well developed in platform-interior, lagoonal-peritidal settings, where facies evolution indicates cyclic deepening and shallowing of the depositional environment. Boundaries of small-scale sequences are commonly accentuated by calcified algal-microbial mats, bird's eyes, desiccation fissures, or calcretes. Karstified surfaces and limonitic crusts appear locally. Early transgressive facies include organic-rich clays, algal-microbial mats, and reworked pebbles. Maximum flooding is suggested by more marine fauna and, in many places, by intensified bioturbation. Early dolomitization is stratabound, which may result from confinement of dolomitizing fluids by clay layers. The lagoonal-peritidal sequences are probably related to climatic and/or eustatic fluctuations in the Milankovitch frequency band. This hypothesis is supported by the cyclical pattern of the downhole logs.

Meter-scale oolite sequences commonly exhibit keystone vugs at their tops, indicating the upper swash zone in a beach environment. Deeper water is suggested by bioturbation. Such sequences can have an autocyclic (dune migration) or allocyclic (sea-level fluctuations) origin.

Small-scale shallowing-upward sequences in Hole 867B illustrate the facies evolution from shoreface to foreshore and to shallow lagoon behind a barrier beach, including washover deposits. The sponge bioherms observed in an offshore setting in Hole 868A grew on erosion surfaces and hardgrounds and were commonly buried or truncated by tempestites. The depositional sequences in these high-energy environments were therefore mostly controlled by storm activity.

The lowermost part of Hole 866A probably was deposited on a shallow ramp, whereas the bulk of the facies represents a generally protected, lagoonal, inner-platform environment. Holes 867B and 868A and the uppermost part of Hole 866A suggest that the platform rim was composed of storm-dominated beach ridges, which protected the lagoon behind them. The sponge-rudist bioherms lived in front of the beach rim and produced carbonate elements that were washed onto the beaches and farther into the lagoon. Abundant carbonate production in the lagoon always maintained shallow water depths. This general facies distribution was modulated by low-amplitude, high-frequency sea-level fluctuations that created the small-scale sequences.

INTRODUCTION

On shallow-water carbonate platforms, sediment accumulation and facies evolution through time are controlled by subsidence, sea-level fluctuations, carbonate productivity, and sediment transport. Classically, sediments form meter-scale shallowing-upward sequences, because the accumulation rates commonly outpace the combined rates of subsidence and sea-level rise (James, 1984). Consequently, the tops of many of these elementary sequences show signs of intertidal to supratidal exposure, or are eroded. Such small-scale sequences are stacked to form larger sequences, which display transgressive or regressive trends of sedimentary facies evolution (here, we use the term "sequence" for a recurring facies succession of any scale that was caused by cyclic, or rather quasi-periodic, processes). Stacking of sequences of various scales has been documented from many ancient carbonate platforms (e.g., Arnaud, 1981; Goodwin and Anderson, 1985; Grotzinger, 1986; Hardie et al., 1986; Strasser, 1988; Arnaud-Vanneau and Arnaud, 1990; Osleger and Read, 1991). The larger-scale facies evolution, in many cases, is related to third-order sea-level fluctuations, whereas the small-scale sequences are commonly attributed to sea-level fluctuations in the Milankovitch frequency band (e.g., Read and Goldhammer, 1988; Goldhammer and Harris, 1989; Goldhammer et al., 1993; Strasser, 1994). This is not surprising, as climatic changes driven by the quasi-periodic perturbations of the Earth's orbit have induced fluctuations of sea level, terrigenous runoff, and carbonate productivity, and thus influenced the sedimentary systems since their earliest existence (Berger et al., 1989; Schwarzacher, 1993). However, in shallow-water depositional environments, autocyclic processes such as migration of bars and islands, delta-switching, and local progradation may also create shallowing-upward sequences and make the interpretation difficult (Strasser, 1991; Goldhammer et al., 1993). Careful facies analysis and correlation of sequences over large distances usually filters out such local effects and may help to identify an orbitally controlled sedimentary record. If absolute age dates are available, the average time represented by one small-scale sequence can be estimated.

During Ocean Drilling Program (ODP) Leg 143, shallow-water carbonates of Hauterivian to Albian age were drilled on Allison and Resolution guyots (Sager, Winterer, Firth, et al., 1993). Although recovery was low on the average (15.1% for Hole 865A on Allison Guyot, 15.4% for Hole 866A, 29.2% for Hole 867B, and 46.3% for

[1] Winterer, E.L., Sager, W.W., Firth, J.V., and Sinton, J.M. (Eds.), 1995. *Proc. ODP, Sci. Results,* 143: College Station, TX (Ocean Drilling Program).

[2] Institut de Géologie, Université de Fribourg, Pérolles, 1700 Fribourg, Switzerland.

[3] Institut Dolomieu, Université de Grenoble, Laboratoire de Géodynamique des Chaînes Alpines, 15 rue Maurice Gignoux, 38031 Grenoble cedex, France.

[4] Laboratoire de Stratigraphie et CNRS-URA 1761, Université Pierre et Marie Curie, 4 place Jussieu, 75252 Paris cedex 05, France.

[5] Bundesanstalt für Geowissenschaften und Rohstoffe, Stilleweg 2, 30655 Hannover, Federal Republic of Germany.

Hole 868A on Resolution Guyot), it is evident from the recovered material, as well as from the downhole logs, that the sedimentary record is composed of meter-scale sequences. This has encouraged us to analyze in detail the facies in the more continuous parts of core, and to study their evolution in terms of high-resolution sequence stratigraphy. We are conscious of the fact that only a part of the facies may have been recovered and that our conclusions, therefore, are biased. Of equal concern is that entire small-scale sequences are missing in the cored material, as evidenced by the analysis of the downhole logs (Cooper et al., this volume). Nevertheless, the sequences found on these Pacific guyots in many ways resemble sequences described from passive margins, where carbonate sediments accumulated in shallow-lagoonal and peritidal settings, or on ooid bars and beaches.

The material presented here comes from Resolution Guyot, where Hole 866A furnished a sedimentary record of 1619 m, ranging from Hauterivian oolitic-oncoidal grainstones of a ramp setting to shallow-lagoonal inner-platform sediments of late Albian age (Fig. 1; Sager, Winterer, Firth, et al., 1993). The sequence-stratigraphic interpretation of this hole is given by Arnaud et al. (this volume). The results from Holes 867B and 868A helped in constructing a transect across the platform rim for the uppermost 60 m of the guyot.

LAGOONAL-PERITIDAL SEQUENCES

A major part of the material recovered from Hole 866A displays facies typical of shallow-lagoonal to peritidal environments (Fig. 1). Where small-scale sequences can be reconstructed, an evolution from intertidal to shallow subtidal and back to intertidal depositional settings is suggested (Figs. 2 through 6). In some cores, there is evidence for subaerial exposure. The general lithologic description was presented by Sager, Winterer, Firth, et al. (1993), and the various types of microfacies encountered are listed by Arnaud et al. (this volume). In the following, only a brief summary of the microfacies will be given, illustrated by some examples relevant to the analyzed sequences.

Subtidal Facies

Most subtidally deposited sediments are wackestones to packstones containing bioclasts and peloids. The fauna includes ostracodes, gastropods, bivalves, and benthic foraminifers (Pl. 1, Figs. 1 and 2). In some samples, these occur almost monospecifically and in large numbers, thus implying a restricted environment. Echinoderms and corals suggesting normal-marine salinity occur only episodically. Dasycladacean algae may be locally abundant. However, they are commonly dissolved and difficult to identify. In some facies, *Cayeuxia* appears sporadically, and unidentified algal or microbial lumps are locally abundant. Oncoids with *Bacinella*-like structures occur in some subtidal facies.

In several sequences, peloids are abundant and form packstones to grainstones, implying a higher energy level. Bioturbation is common.

Intertidal Facies

Intertidal exposure is indicated by the presence of bird's-eye vugs and desiccation fissures in mudstones, wackestones, and packstones (Pl. 1, Figs. 3 and 4).

Algal-microbial Mat Facies

Characteristic features of the peritidal facies in Hole 866A are the abundant algally and/or microbially constructed facies. Thrombolitic frameworks suggest predominantly subtidal formation, where space for growth was available (Pl. 1, Figs. 5 and 6), whereas laminated algal-microbial mats with bird's eyes point to an intertidal setting. Some algal structures resemble *Hormathonema,* described by Masse (1979) from the Barremian in France (Pl. 2, Fig. 1). *Girvanella* locally contributes to the binding of sediment.

In many samples, spherulites of probably microbial origin (Chafetz, 1986) compose a large part of the algal-microbial facies (Pl. 2, Figs. 2 and 4). They are locally associated with framboidal pyrite (Pl. 2, Fig. 3), which probably formed when bacteria decomposed the organic matter (Monty, 1981). Dolomite formation in these facies may also be microbially induced (Monty et al., 1987).

The good preservation of these algal-microbial facies points to early cementation. This is confirmed by the common reworking of algal chips at the base of the overlying sequences (Fig. 4). Calcification of cyanobacteria can begin during the life of the organisms, or can take place within a few months after their death (Riding, 1991, p. 79).

Clays and Organic Matter

Clay seams appear repeatedly in subtidal and intertidal facies. They are composed mostly of illite and interstratified illite/smectite minerals; chlorite and kaolinite are subordinate. Iron-rich neoformed illite has been identified in some clay fractions (Baudin et al., this volume). These illites are similar to those described from peritidal and lacustrine settings in the lowermost Cretaceous (Purbeckian) of France and Switzerland, where they probably formed through repeated emersion-immersion cycles (Deconinck and Strasser, 1987).

Organic matter commonly is associated with the clays and contains still recognizable terrestrial debris such as organic sheaths and pieces of wood. Nevertheless, the bulk of the organic matter has a bacterial or algal origin and is concentrated in finely laminated black layers. This facies is well developed in Units IV and VI and has total organic-carbon (TOC) contents reaching 34% in Core 143-866A-85R (Baudin et al., this volume).

Dolomitization

Dolomitization of peritidal facies is of early-diagenetic origin, as suggested by small crystal sizes and patchy, facies-dependent distribution (Röhl and Strasser, this volume). Small, mostly euhedral dolomite crystals are disseminated in the sediment, or concentrated above clay seams (Pl. 2, Fig. 5). This latter observation suggests that dolomitizing fluids may have been confined by the impermeable clay layers, which led to stratabound early dolomitization (Figs. 5 and 6). Later-stage pervasive dolomitization dominates in the lower part of Hole 866A (Units VII and VIII; Flood and Chivas, this volume).

Subaerial Exposure

In several samples, subaerial exposure and vadose diagenesis are evident (see also Röhl and Strasser, this volume). Meniscus cements and pedogenetic glaebules (Pl. 2, Fig. 6), as well as circum-granular cracking (Esteban and Klappa, 1983), are typical features. Calcrete appears in the upper part of the hole (Fig. 1; Sager, Winterer, Firth, et al., 1993), but recovery there was not sufficient to permit the reconstruction of small-scale sequences.

Interpretation in Terms of High-Resolution Sequence Stratigraphy

Many of the observed meter-scale sequences display first deepening-upward, then shallowing-upward trends in facies evolution, and they are commonly capped by intertidal to supratidal exposure surfaces. Thus, they can be interpreted in terms of sequence stratigraphy (Vail, 1987): emersion surfaces are termed sequence boundaries (SB), and surfaces directly underlying deeper facies are called transgressive surfaces (TS). Relatively deepest water environment (MF = maximum flooding) commonly is not indicated by a surface but by a specific facies association, by intensified bioturbation suggesting lower sedimentation rates, or by a concentration of organic matter. Because the geometry of the sedimentary bodies is not known, it is of course not possible to identify systems tracts in these small-scale

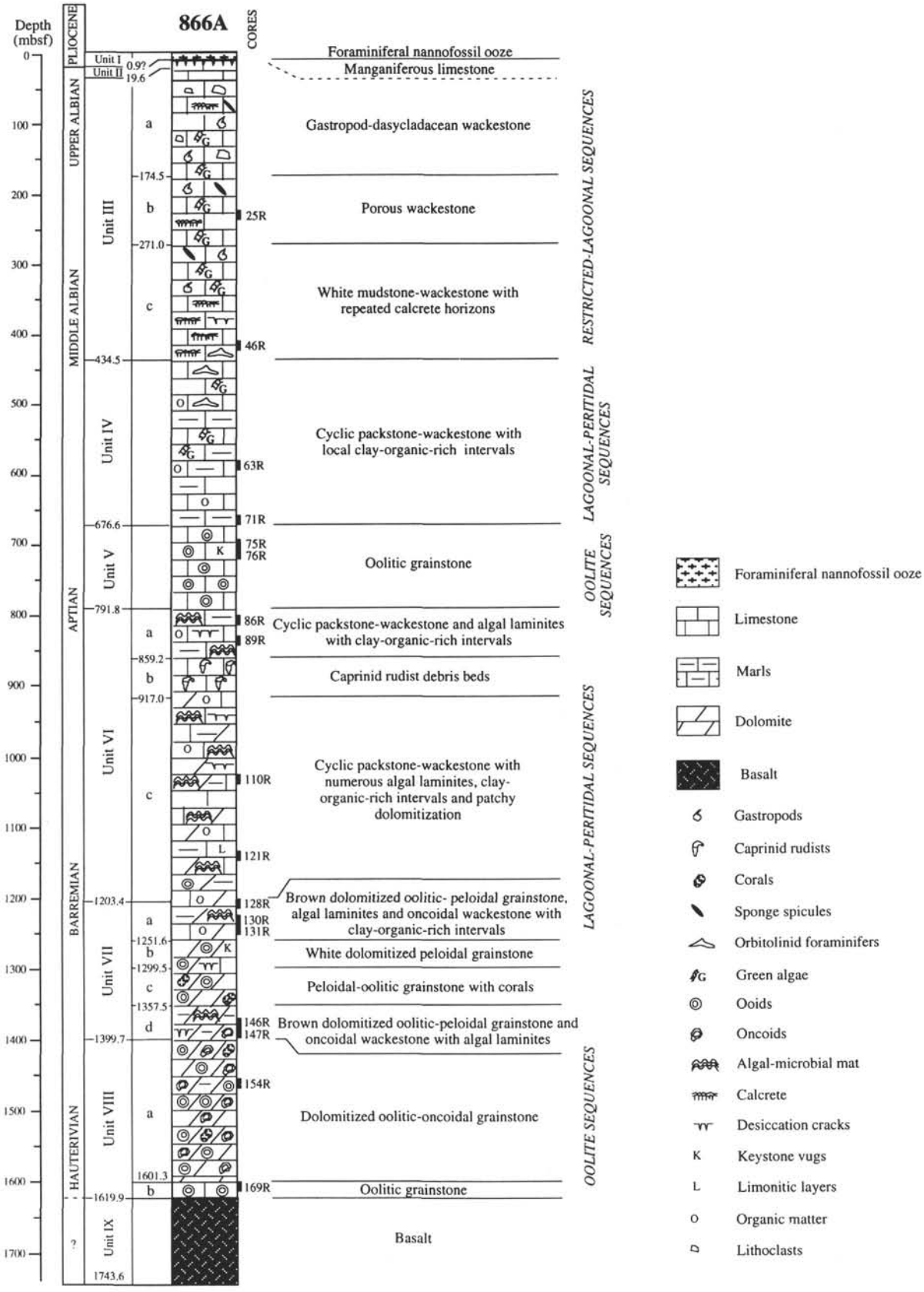

Figure 1. Summary of Hole 866A with distribution of predominant small-scale sequence types (modified from Sager, Winterer, Firth, et al., 1993). Locally, small-scale sequences are difficult to identify owing to low recovery, but are inferred from recovered facies and the cyclic pattern in downhole logs. The cores illustrated in Figures 2 through 7 are labeled, as well as the cores from which photomicrographs are presented (Pls. 1–3).

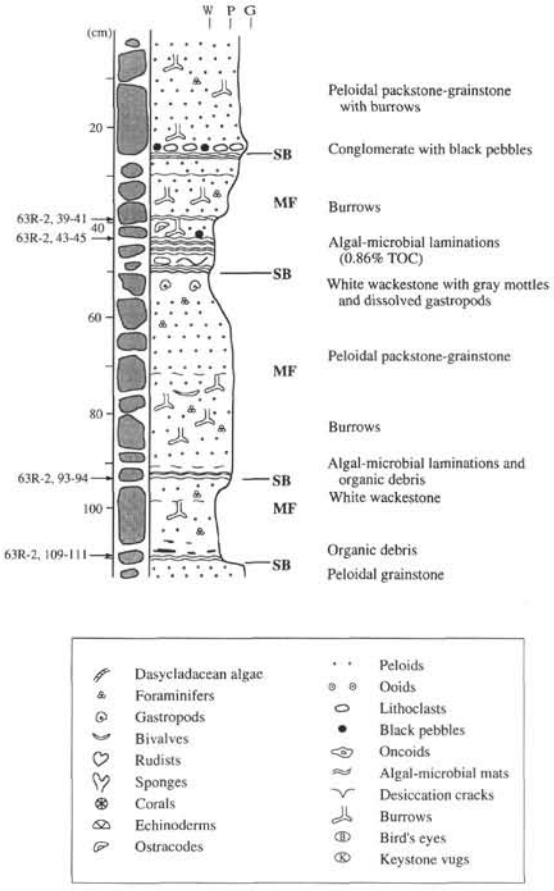

Figure 2. Lagoonal-peritidal sequences interpreted from material recovered in Section 143-866A-63R-2. Recovered rock fragments are marked in left column. As important parts of core between the fragments may be missing (recovery was 23.1%), some facies may have been washed out, and the actual small-scale sequences may be much thicker. Small-scale sequence boundaries are marked SB; facies suggesting deepest water and/or slower sedimentation rates imply maximum flooding (MF). Interpretation is based on sketches made directly from the core and on thin sections (marked on left). Dunham-classification: M = mudstone, W = wackestone, P = packstone, G = grainstone, F = floatstone, R = rudstone, B = boundstone; TOC = total organic carbon.

sequences. Nevertheless, in this study we prefer to apply the concept of third-order sequences of Vail (1987), rather than using the parasequence concept (Van Wagoner et al., 1990), because the observed sequences, in most cases, are bounded by emersion surfaces, not by marine flooding surfaces.

In the small-scale sequences presented here (Figs. 2 through 6), sequence boundaries appear at the end of a generally continuous shallowing-upward facies evolution, terminating in bird's eyes, calcified algal-microbial mats, or desiccation cracks. Limonitic clays may have formed at the end of a shallowing-upward phase (late highstand), or they may represent lowstand deposits (Fig. 5). Pseudomorphs of anhydrite and gypsum have been found in several cores (Arnaud et al., this volume).

In most cases, transgressive deposits directly overlie the sequence boundaries, because in such shallow depositional environments there was no space available to accommodate lowstand deposits. In an early stage, transgression reworked the material that had been exposed previously, leading to conglomerates composed of rip-up clasts and algal chips. Clays had the greatest potential to be eroded and transported from the hinterland when relative sea level was low, and/or when rainfall was abundant. They generally bypassed the platform during low sea level, but accumulated during the early flooding

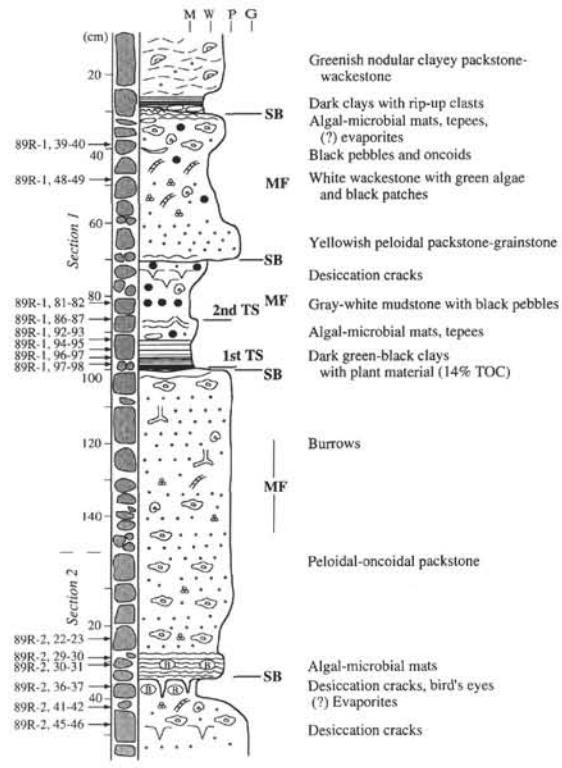

Figure 3. Lagoonal-peritidal sequences in Core 143-866A-89R. Recovery was 18.8%. TS = transgressive surface; other labels and symbols as in Figure 2.

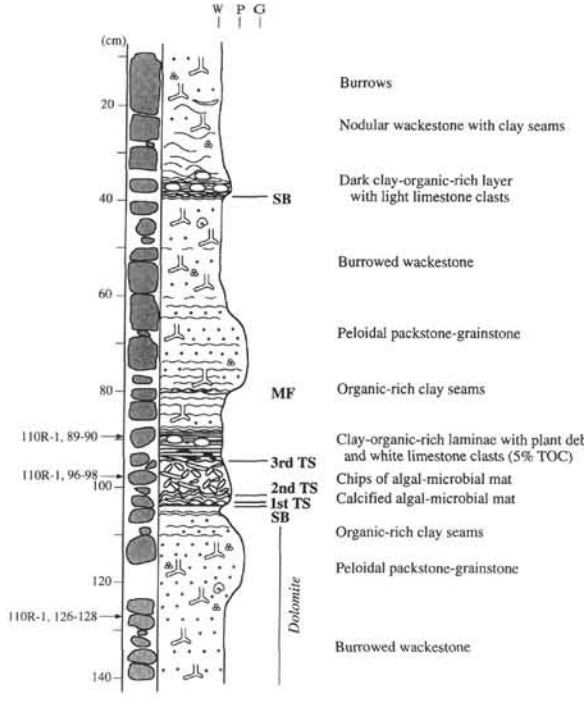

Figure 4. Lagoonal-peritidal sequences in Section 143-866A-110R-1. Recovery was 25%. See Figures 2 and 3 for further explanation.

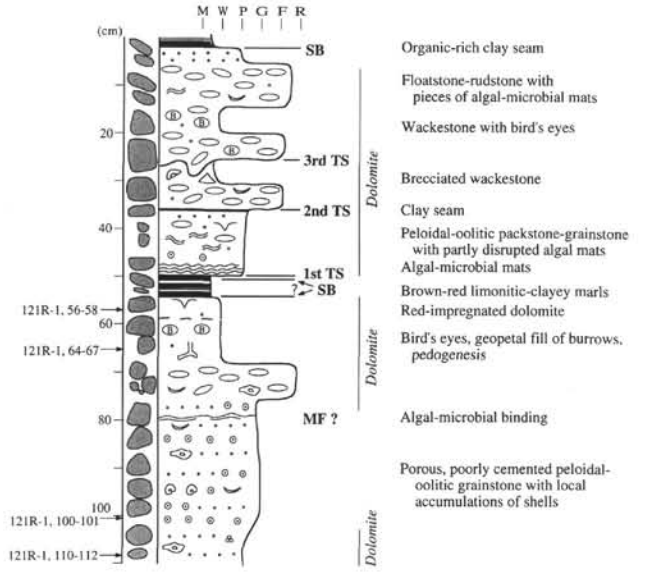

Figure 5. Partly dolomitized lagoonal-peritidal sequences in Section 143-866A-121R-1. Recovery was 8.6%. High-energy deposits are locally characterized by erosive transgressive surfaces. Dolomitization appears to be stratabound. For further explanations, refer to Figures 2 and 3.

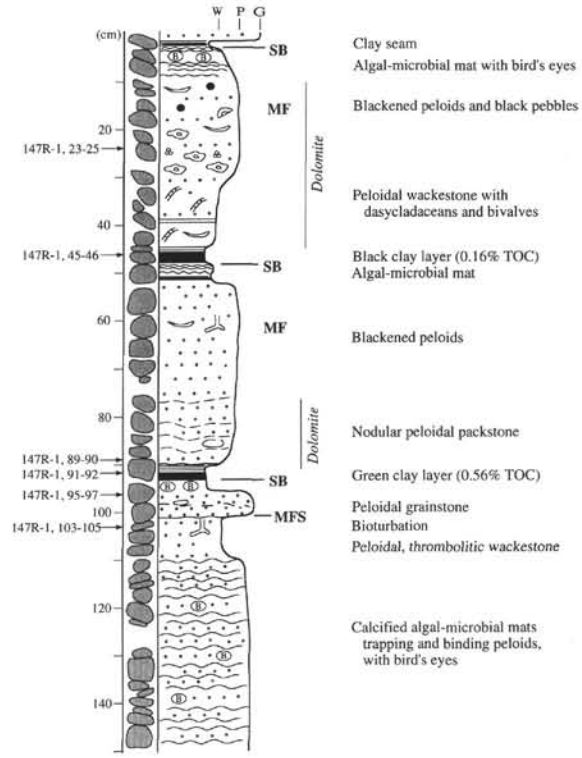

Figure 6. Partly dolomitized lagoonal-peritidal sequences in Section 143-866A-147R-1. Recovery was 28.9%. Dolomitization appears to be stratabound and confined by clay seams. MFS = maximum-flooding surface. For other labels and symbols, refer to Figure 2.

phases. They probably settled in shallow ponds before water depth was sufficient for the proliferation of carbonate-producing organisms. Reworked terrestrial organic matter was mixed with marine organic matter (Baudin et al., this volume). As water depth increased and carbonate production set in, the organic matter was rapidly covered and thus protected from oxidation. In some cores (Figs. 3, 4, and 5), multiple transgressive surfaces can be recognized, which locally resemble ravinement surfaces (Fig. 5). This is explained by a threshold effect, by which calm lagoons are instantly flooded and exposed to higher energy once sea level has risen enough to pass over barrier islands. Black pebbles have been encountered in several sequences. They formed through the impregnation of subtidal, intertidal, or supratidal carbonate sediment by organic matter, which stimulated rapid cementation, or through forest fires (Strasser, 1984; Shinn and Lidz, 1988). Reworking then led to the formation of pebbles that generally appear in transgressive deposits, but can also be found dispersed in other facies. Algal-microbial mats are typical of tidal flats in a transgressive context (Shinn, 1983). As water depth increased, they formed thrombolitic structures.

Relatively deepest water depths in the evolution of a small-scale sequence and/or lowest sedimentation rates owing to rapid increase of water depth are implied by lagoonal fauna and flora and by intense bioturbation. Clays and organic matter may locally be concentrated (Fig. 4). In Core 143-866A-147R (Fig. 6), peloidal grainstone overlies bioturbated wackestone with a sharp contact that has been interpreted as a maximum-flooding surface (MFS). During relative sea-level highstand, the lagoon was then gradually filled to the intertidal level.

Above the interval of maximum flooding, facies evolution generally shows a shallowing-upward trend that leads to the next sequence boundary. In many of the studied sequences, these small-scale highstand deposits are relatively thin in comparison with the transgressive parts of the sequences (Figs. 2 and 6). This may result from the shallow depositional environments on the platform top, where accommodation space is created mostly during accelerating relative sea-level rise in the transgressive phase, but is rapidly lost when carbonate sediment fills the available space during decreasing rates of sea-level rise during highstand.

Early dolomitization, in some cases, is related to intertidal facies and could have been initiated penecontemporaneously. However, it also affected subtidal sediments, suggesting that dolomitizing fluids percolated through the entire sequence. These fluids may have been ponded by clay layers at the base of the sequences (Figs. 5 and 6). It is reasonable to propose a model of flood recharge and evaporative pumping, in which marine waters mixed with fresh water during periodic flooding of tidal flats and were then concentrated to the dolomite saturation level (Müller et al., 1990). Concentrations were only at times sufficiently elevated to allow for the precipitation of gypsum or anhydrite.

The calcretes in Unit III (Fig. 1) imply emersion for a relatively long period of time and are good indicators of small-scale sequence boundaries. However, recovery was too low to permit the reconstruction of small-scale sequences. The recovered material, including the calcretes, possibly represents diagenetic caps, and the only weakly cemented sediment making up the bulk of the sequences was washed out during drilling. The recovered facies suggest a restricted lagoonal environment.

Small-scale carbonate sequences in peritidal settings can form through allocyclic or autocyclic processes (Strasser, 1991). High-frequency allocyclic sea-level fluctuations are typically related to climatic cycles induced by perturbations of the Earth's orbit (Milankovitch, 1941; Hays et al., 1976; Berger et al., 1989). In times such as the Early Cretaceous when polar ice-caps were absent or much reduced (Frakes and Francis, 1988), volume changes of Alpine glaciers (Fairbridge, 1976), changes in lake and groundwater storage (Jacobs and Sahagian, 1993), thermal expansion of the ocean surface (Gornitz et al., 1982), and/or geoidal changes (Mörner, 1994) are sufficient to create sea-level fluctuations of a few meters amplitude. Such fluctuations can easily produce small-scale sequences of the type observed on Resolution Guyot as well as on many passive margins (Strasser, 1994). Autocyclic processes include progradation of tidal flats (Ginsburg, 1971), lateral migration of shoals and islands (Pratt and James, 1986), or migration of tidal inlets and channels. Differential compaction may create locally increased subsidence

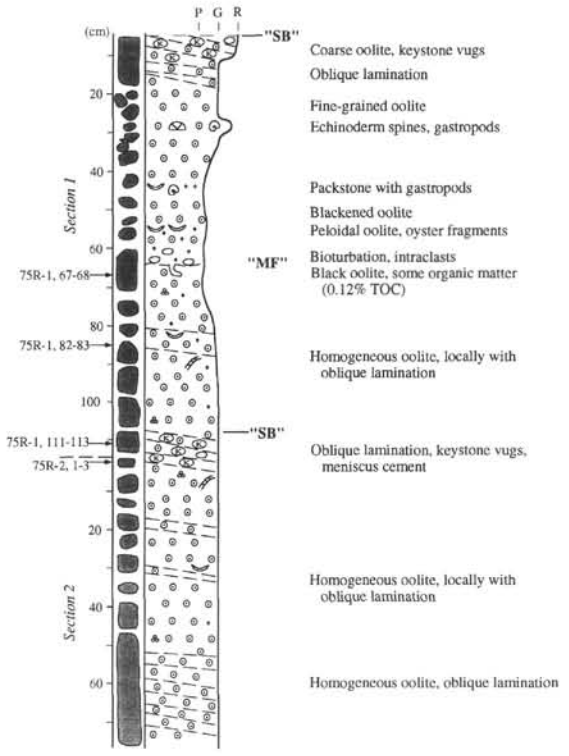

Figure 7. Oolitic sequences in Core 143-866A-75R. Recovery was 41.8%. Because these sequences may also have an autocyclic origin, the labels for sequence boundaries and maximum flooding have been placed in quotation marks. For more explanations, see Figure 2.

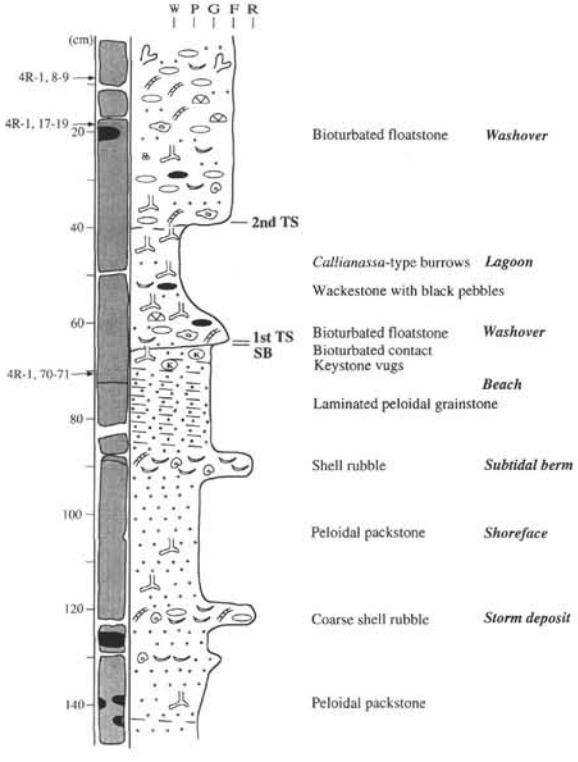

Figure 8. Storm-beach sequences in Section 143-867B-4R-1. Recovery was 73.4%. Black areas in left column are dissolution cavities in the core that are partly filled with phosphatic internal sediment. For more explanations, see Figures 2 and 3.

rates and lead to transgressions independent of a general sea-level rise (van Waasbergen and Winterer, this volume).

Based on the facies analysis of one borehole only with limited recovery, it is difficult to evaluate if the sequences presented here have allocyclic or autocyclic origins. Karstification and pedogenesis directly overlying and overprinting subtidal facies have been noted in several cores from Hole 866A (e.g., Sections 130R-1, 105–107 cm; -132R-1, 25–30 cm; -138R-1, 10–25 cm). Such features can develop only when relative sea level drops below the surface of the previously deposited sediment, thus implying allocyclic sea-level fluctuations or tectonic uplift. Spectral analysis of the resistivity and gamma-ray logs, however, revealed cyclic patterns that clearly suggest an orbital control of these sequences, with periodicities corresponding to obliquity and eccentricity (Cooper, this volume). Owing to low recovery, it is not possible to attribute the observed small-scale sequences to a particular periodicity. Sequences related to the precession of the equinoxes may be present in the recovered material, but the vertical resolution of the downhole logs is not high enough to pick them out. Furthermore, autocyclic processes may locally have been superimposed.

OOLITE SEQUENCES

In Hole 866A, Units V and VIII and parts of Unit VII are dominated by oolites (Fig. 1; Sager, Winterer, Firth, et al., 1993; Arnaud et al., this volume; Jenkyns and Strasser, this volume). In some cores, small-scale sequences could be defined, one of which is presented in Figure 7. Keystone vugs, implying the intertidal swash zone, define the shallowest part of the sequence, whereas bioturbation, concentration of fossils, and blackening resulting from finely dispersed organic matter would suggest the relatively deepest part. Grainstone facies and planar, oblique laminations formed on beaches and sand bars exposed to high water energy; packstones formed in quieter water.

Early marine cementation by a fringing cement stabilized the sediment. A second-generation blocky calcite cement (Pl. 3, Fig. 1) suggests the influence of freshwater, which percolated freely through the porous and permeable grainstones and which could be recharged from rains onto emergent sand bars and islands (Röhl and Strasser, this volume). If freshwater cementation did not take place, overpacking occurred (Pl. 3, Fig. 2).

It is not possible to apply the sequence-stratigraphic concept to the oolite sequences. They could have formed by fluctuations of relative sea level in the same way as the peritidal sequences (allocyclic origin), but also through the lateral migration of sand bars and islands (autocyclic origin).

STORM-BEACH SEQUENCES

In the upper part of Hole 867B, storm and beach deposits predominate (Sager, Winterer, Firth, et al., 1993). Core 143-867B-4R displays an upward succession from shoreface to beach to washover deposits (Fig. 8). The foreshore facies is punctuated by a storm layer of coarse shell rubble. The passage from shoreface to beach laminations is again characterized by shell rubble, which can be interpreted as a subtidal berm where the waves break and a vortex is created. The upper beach facies contains keystone vugs. Shoreface sediment overlying the beach facies was deposited by a storm washover; the base of this deposit is interpreted as a transgressive surface. Above it, facies change to lagoonal and show abundant bioturbation, which also cuts through the transgressive surface (Fig. 8). A second washover deposit finally covers the lagoon.

Echinoderms, dasycladacean algae, and gastropods indicate a more open-marine environment and normal salinity. High-energy facies formed on the exposed shoreface and foreshore, and are represented by grainstones and rudstones (Pl. 3, Fig. 3). Behind the beach ridge, lagoonal sediments and washover deposits are composed of packstones and floatstones (Pl. 3, Fig. 4).

In such storm-dominated environments, transgressive surfaces are the major sequence-stratigraphic elements. In front of the beach rim they were erosive (ravinement surfaces), whereas in the lagoon they formed the base of aggrading washover deposits.

SPONGE-RUDIST BIOHERM SEQUENCES

In Hole 868A, bioherm facies composed of rudists, sponges and corals were recovered (Sager, Winterer, Firth, et al., 1993). In particular, Core 143-868A-2R shows a succession of constructed framestones to bafflestones (Pl. 3, Figs. 5 and 6), interrupted by floatstones to packstones or wackestones (Fig. 9). Bioherms may be almost monospecific (sponges or requieniid rudists; Swinburne and Masse, this volume), or may be composed of different faunal groups. Corals generally are subordinate. In some cores, the bioherms display an evolution through time from larger to smaller individuals, or from one sponge type to another.

The bioherms commonly grew on erosive surfaces that are interpreted as small-scale sequence boundaries and/or transgressive surfaces. The top of a bioherm may show dissolution features and borings. Such hardgrounds are attributed to maximum-flooding surfaces, where no sediment was deposited for some time. The overlying floatstones to wackestones containing broken branches of sponges would then represent the highstand deposits.

These sequences formed on the slope, in water depths of a few tens of meters. The bioherms were exposed to wave and storm action, but possibly were affected also by relative sea-level fluctuations. Sedimentation was interrupted when sea level rose rapidly, thus producing hardgrounds. A slowing rise of sea level would then permit progradation of sediment over the bioherms. A drop in sea level caused the storm-wave base to be lowered, creating erosive surfaces.

TOWARD A DEPOSITIONAL MODEL

Sequence-stratigraphic analysis of Hole 866A (Arnaud et al., this volume) suggests that the sedimentary history of Resolution Guyot began with marine oolitic-oncolitic sand sheets forming on a ramp. These facies shallow upward and show a terrestrial input of clays and lignite. At about 1400 mbsf (close to the boundary between Units VIII and VII; Fig. 1), a karst surface separates the ramp succession from the inner-platform facies. The lagoonal-peritidal sequences described above form the major building blocks of a basically aggradational succession, which is sporadically punctuated by more open-marine facies: corals and ooids in Unit VII, rudists in Unit VI, and ooids again in Unit V.

Clays are absent above 500 mbsf (Fig. 1), suggesting that during deposition of Unit IV the volcanic edifice was progressively covered by the carbonate platform. However, the seismic data of Resolution Guyot show flat and continuous reflectors down to depths corresponding to Unit VI (Sager, Winterer, Firth, et al., 1993). This could mean that only isolated volcanic structures were emerging that have not been crossed by the seismic lines, and/or that clay minerals have been washed in from nearby, still emergent volcanic edifices (E.L. Winterer, pers. comm., 1994).

Algal-microbial mat facies dominate Units VII and VI, whereas calcretes are found in Unit III. The depositional environments of these units were generally very shallow and probably controlled by small-amplitude, high-frequency sea-level fluctuations. The different sedimentary expressions may have several reasons. During the deposition of Units VII and VI, the climate probably was more humid owing to the catchment of clouds by the volcanic relief, and/or a paleolatitudinal position in a low-pressure climatic zone. On the other hand, the presence of early-diagenetic dolomite and the local occurrences of evaporites imply periods of higher groundwater salinities, which may also have favored the growth of algal-microbial mats. Therefore, a strongly seasonal climate must be postulated that controlled the sedimentation together with high-frequency sea-level fluctuations.

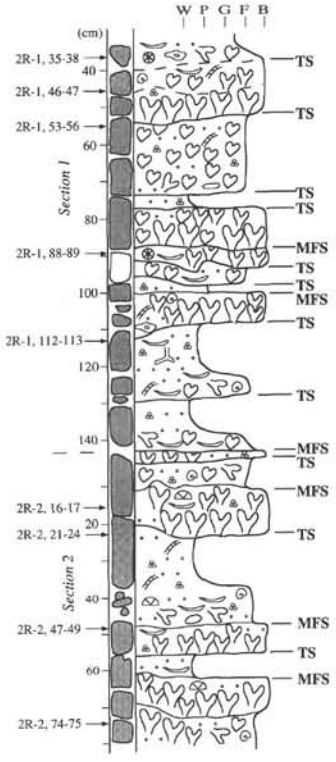

Figure 9. Sponge-rudist bioherm sequences in Core 143-868A-2R. Recovery was 68%. Surfaces are either erosional, and thus interpreted as storm-induced transgressive surfaces (TS), or represent hardgrounds, suggesting maximum-flooding surfaces (MFS). Rock fragment left white is a whole-round sample. For other explanations, refer to Figure 2.

During deposition of Unit III, the climate probably was semiarid, which led to the formation of calcretes (Esteban and Klappa, 1983). Evaporation, evapotranspiration, and CO_2-degassing were the main factors in calcrete formation (Wright and Tucker, 1991), but conditions were never suitable for precipitation of dolomite and evaporites. Furthermore, sea-level fluctuations of a higher amplitude may have periodically exposed the sediment surface for a longer time and allowed for calcrete formation, whereas in Units VII and VI generally lower amplitudes favored the development of tidal flats.

The uppermost 60 m of Hole 866A, Hole 867B and Hole 868A can be used to reconstruct the platform rim during late Albian time (Fig. 10). The surface appearing on the 3.5-kHz echo-sounder profile (Sager, Winterer, Firth, et al., 1993) corresponds to the phosphate-manganese crust that formed after karstification of the platform surface. However, it is reasonable to assume that Hole 867B is situated on the original rim of the platform, and Hole 866A in a protected lagoon behind.

Facies from the uppermost part of Hole 866A suggest a shallow-lagoonal setting with sporadic washovers. The base of Hole 867B shows shallow lagoonal facies with some rudists, which pass upward into ooid sands and then into the storm-dominated and high-energy intertidal facies described above. This vertical evolution implies that the platform rim must have migrated from north to south (i.e., toward the platform interior), which suggests a general transgressive trend. This is consistent with the evolution toward more marine faunas in the top of Unit III, Hole 866A (Sager, Winterer, Firth, at al., 1993, Chapter 7, Fig. 30). Before final drowning, however, a drop of relative sea level led to significant karstification of the platform top in the late Albian (Sager, Winterer, Firth, et al., 1993), as it has also been documented from other Mid-Pacific guyots (e.g., Winterer and Metzler, 1984; Grötsch and Flügel, 1992).

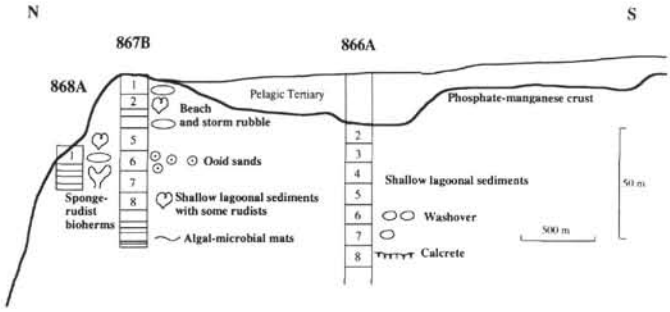

Figure 10. General facies interpretation of Hole 867B on the platform rim, Hole 868A on a terrace 33 m deeper and 400 m to the north, and of the uppermost part of Hole 866A, 1.6 km toward the platform interior. Topography is based on a 3.5-kHz echo-sounder profile (Sager, Winterer, Firth, et al., 1993, Chapter 7, Fig. 6). For discussion refer to text.

Hole 868A is situated some 400 m to the north of the rim and some 33 m deeper. Sponge-rudist bioherms of the kind described above characterize the recovered cores. Material produced by this reef community was reworked by storm and wave action, accumulated on the platform rim to form beaches and islands, and was exported into the lagoon by washovers.

This geometrical reconstruction implies that the platform rim was not formed by a reef framework as on modern atolls, but rather by storm beaches and islands that protected a shallow lagoon behind (Fig. 10). Similar depositional profiles have been described from the Lower Cretaceous of France by Arnaud (1981), from Upper Cretaceous rudist buildups in Italy by Carbone and Sirna (1981), and from mid-Cretaceous rudist reefs in Israel by Ross (1992). Alternatively, reconstructions of the mid-Cretaceous El Abra platform in Mexico (Enos 1974, 1986; Minero, 1991), the Comanche shelf margin in Texas (Scott, 1990), and Cretaceous coral-rudist bioherms in France (Masse and Philip, 1981) show the bioherms positioned closer to the platform rim, but equally associated with high-energy bioclastic and oolitic deposits. The facies sequences identified in Hole 866A resemble those from the platform interior in El Abra, where Enos (1986) and Minero (1991) described meter-scale depositional sequences of shallow lagoonal and tidal-flat facies terminating with subaerial exposure surfaces including calcrete and microkarst.

Carbonate production of the sponge-rudist bioherms was sufficient to maintain active accumulation of the beach rim for most of the time, and only occasional rapid relative sea-level rises allowed an opening of the lagoon. Carbonate production in the lagoon itself was such that water depths stayed shallow through most of the depositional history. Small-amplitude, high-frequency sea-level fluctuations in the Milankovitch frequency band (Cooper, this volume) modulated the sedimentation pattern in the shoreface, foreshore and lagoonal settings, but were most effective in creating small-scale sequences in the protected platform interior. The shoreface and foreshore were dominated mainly by storm activity. Sea-level cycles not only controlled sedimentation through changes in water depth, but may also have induced cycles in nutrient flux, which in turn influenced the growth pattern of the bioherms (Hallock and Schlager, 1986; Scott, 1988).

Subsidence rates were probably comparable to those of passive margins. If the 1619 m of sediment in Hole 866A are estimated to span the late Hauterivian to late Albian (Fig. 1), that is, about 35 Ma (Harland et al., 1990), the average subsidence rate would be about 0.046 mm/yr. This rate does not take into account possible time gaps or compaction, but is comparable to values of 0.05 to 0.1 mm/yr for mature passive margins (Grotzinger, 1986).

The facts that (1) only one deep hole has been drilled through the entire carbonate platform, (2) only one small part on the rim of Resolution Guyot could be reconstructed in two dimensions, and (3) recovery was low forestalls any advanced conclusions about the evolution of the entire edifice. The seismic-reflection profiles (Sager, Winterer, Firth, et al., 1993, Chapter 7, Figs. 7 and 9) do not show sufficient detail to interpret sedimentary systems tracts and to establish a sequence-stratigraphic framework valid for the entire guyot. Also, it is possible that during the evolution of the platform rim there was a difference between the windward and leeward margins, as observed on modern atolls (e.g., Harmelin-Vivien, 1985). Nevertheless, the general sequence-stratigraphic trends reconstructed for Hole 866A are comparable to those of time-equivalent carbonate platforms in the Tethyan realm, suggesting that eustatic sea-level fluctuations on the million-year scale were at least partly responsible for the evolution of Resolution Guyot (Arnaud et al., this volume).

It is striking to see that the overall facies evolution recorded in Hole 866A compares very well with the one found in Hole 865A on Allison Guyot. Although the guyots formed at different times, and despite different subsidence rates (Jenkyns, this volume), the basic principles of platform growth seem to be the same. However, to understand the anatomy and the life history of Pacific guyots, one would have to drill several holes on one single guyot, situated on a transect from the windward margin through the center and on to the leeward margin. Every guyot has its own life cycle, but possibly a Pacific-wide eustatic and/or tectonic control set the stage for a common destiny.

CONCLUSIONS

Analysis of the material recovered in Holes 866A, 867B, and 868A on Resolution Guyot revealed the presence of small-scale sedimentary sequences that formed in different depositional environments. Lagoonal-peritidal sequences in the lower part of Hole 866A display abundant algal-microbial mat facies possibly related to a seasonally humid climate, whereas calcretes capping restricted-lagoonal sequences would have formed in a semiarid climate. The genesis of these quiet-water sequences was most probably related to low-amplitude, high-frequency sea-level fluctuations in the Milankovitch frequency band (Cooper, this volume). Autocyclic processes may have been superimposed.

Ooid sequences imply higher water energy and a more open-marine influence. They may have formed through allocyclic and/or autocyclic processes such as the migration of ooid sand bars.

Hole 867B was drilled on the platform rim and displays high-energy deposits in its upper part. The sequences here are dominated by storm and beach facies, and by washover fans in a protected lagoon. Hole 868A is situated seaward of the platform rim and contains sponge-rudist bioherms. Their growth was periodically interrupted by erosion or by the formation of hardgrounds, which may have resulted from storm and wave action as well as from fluctuating sea level.

The picture emerging from these three holes is that of a platform where, from the Hauterivian through to the late Albian, carbonate production could always keep pace with increasing accommodation space, created by both subsidence and eustatic sea-level rise. Facies therefore always stayed shallow, but were sporadically punctuated by more open-marine influences. The uppermost, marginal part of the guyot reveals a rim formed by storm-beach ridges that protected a shallow lagoonal environment behind them. This is in contrast to modern atolls, where the rim is formed mainly by a reef framework.

ACKNOWLEDGMENTS

We thank all the participants of Leg 143 who made it possible to admire each piece of rock coming up, and who helped to elaborate some of the hypotheses presented here. A.S. acknowledges the financial support of the Swiss National Science Foundation, U.R. that of the German Research Foundation. We also thank P. Dietsche for the preparation of the thin sections, and D. Cao for the SEM photography. The thoughtful and constructive reviews by R.W. Scott, J.F. Read, and E.L. Winterer greatly improved the manuscript.

REFERENCES*

Arnaud, H., 1981. De la plate-forme urgonienne au bassin vocontien: le Barrémo-Bédoulien des Alpes occidentales entre Isère et Buëch (Vercors méridional, Diois oriental et Dévoluy). *Géol. Alp., Mém. Spéc.,* 11.

Arnaud-Vanneau, A., and Arnaud, H., 1990. Hauterivian to Lower Aptian carbonate shelf sedimentation and sequence stratigraphy in the Jura and northern Subalpine chains (southeastern France and Swiss Jura). *In* Tucker, M.E., Wilson, J.L., Crevello, P.D., Sarg, J.R., and Read, J.F. (Eds.), *Carbonate Platforms: Facies, Sequences and Evolution.* Spec. Publ. Int. Assoc. Sedimentol., 9:203–233.

Berger, A., Loutre, M.F., and Dehant, V., 1989. Astronomical frequencies for pre-Quaternary palaeoclimate studies. *Terra Nova,* 1:474–479.

Carbone, F., and Sirna, G., 1981. Upper Cretaceous reef models from Rocca di Cave and adjacent areas in Latium, central Italy. *In* Toomey, D.F. (Ed.), *European Fossil Reef Models.* Spec. Publ.—Soc. Econ. Paleontol. Mineral., 30:427–445.

Chafetz, H.S., 1986. Marine peloids: a product of bacterially induced precipitation of calcite. *J. Sediment. Petrol.,* 56:812–817.

Deconinck, J.F., and Strasser, A., 1987. Sedimentology, clay mineralogy and depositional environment of Purbeckian green marls (Swiss and French Jura). *Eclogae Geol. Helv.,* 80:753–772.

Enos, P., 1974. Reefs, platforms, and basins of Middle Cretaceous in northeast Mexico. *AAPG Bull.,* 58:800–809.

————, 1986. Diagenesis of mid-Cretaceous rudist reefs, Valles Platform, Mexico. *In* Schroeder, J.H., and Purser, B.H. (Eds.), *Reef Diagenesis:* Berlin (Springer), 160–185.

Esteban, M., and Klappa, C.F., 1983. Subaerial exposure environment. *In* Scholle, P.A., Bebout, D.G., and Moore, C.H. (Eds.), *Carbonate Depositional Environments.* AAPG Mem., 33:1–54.

Fairbridge, R.W., 1976. Convergence of evidence on climatic change and ice ages. *Ann. N.Y. Acad. Sci.,* 91:542–579.

Frakes, L.A., and Francis, J.E., 1988. A guide to Phanerozoic cold polar climates from high-latitude ice rafting in the Cretaceous. *Nature,* 333:547–549.

Ginsburg, R.N., 1971. Landward movement of carbonate mud: new model for regressive cycles in carbonates. *AAPG Bull.,* 55:340. (Abstract)

Goldhammer, R.K., and Harris, M.T., 1989. Eustatic controls on the stratigraphy and geometry of the Latemar buildup (Middle Triassic), the Dolomites of northern Italy. *In* Crevello, P.D., Wilson, J.L., Sarg, J.F., and Read, J.F. (Eds.), *Controls on Carbonate Platform and Basin Development.* Spec. Publ.—Soc. Econ. Paleontol. Mineral., 44:323–338.

Goldhammer, R.K., Lehmann, P.J., and Dunn, P.A., 1993. The origin of high-frequency platform carbonate cycles and third-order sequences (Lower Ordovician El Paso Gp, west Texas): constraints from outcrop data and stratigraphic modeling. *J. Sediment. Petrol.,* 63:318–359.

Goodwin, P.W., and Anderson, E.J., 1985. Punctuated aggradational cycles: a general hypothesis of episodic stratigraphic accumulation. *J. Geol.,* 93:515–533.

Gornitz, V., Lebedeff, S., and Hansen, J., 1982. Global sea level trend in the past century. *Science,* 215:1611–1614.

Grötsch, J., and Flügel, E., 1992. Facies of sunken Early Cretaceous atoll reefs and their capping late Albian drowning succession (northwestern Pacific). *Facies,* 27:153–174.

Grotzinger, J.P., 1986. Upward shallowing platform cycles: a response to 2.2 billion years of low-amplitude, high-frequency (Milankovitch band) sea level oscillations. *Paleoceanography,* 1:403–416.

Hallock, P., and Schlager, W., 1986. Nutrient excess and the demise of coral reefs and carbonate platforms. *Palaios,* 1:389–398.

Hardie, L.A., Bosellini, A., and Goldhammer, R.K., 1986. Repeated subaerial exposure of subtidal carbonate platforms, Triassic, northern Italy: evidence for high frequency sea level oscillations on a 10^4 year scale. *Paleoceanography,* 1:447–457.

Harland, W.B., Armstrong, R.L., Cox, A.V., Craig, L.E., Smith, A.G., and Smith, D.G., 1990. *A Geologic Time Scale 1989:* Cambridge (Cambridge Univ. Press).

Harmelin-Vivien, M., 1985. Atoll de Tikehau, archipel des Tuamotu. *In* Delesalle, B., Galzin, R., and Salvat, B. (Eds.), *Proc. 5th Int. Coral Reef Congress Tahiti,* 1:213–256.

Hays, J.D., Imbrie, J., and Shackleton, N.J., 1976. Variations in the Earth's orbit: pacemaker of the ice ages. *Science,* 194:1121–1132.

Jacobs, D.K., and Sahagian, D.L., 1993. Climate-induced fluctuations in sea level during non-glacial times. *Nature,* 361:710–712.

James, N.P., 1984. Shallowing-upward sequences in carbonates. *In* Walker, R.G. (Ed.), *Facies Models* (2nd ed.). Geosci. Can. Reprint Ser., 1:213–228.

Masse, J.-P., 1979. Schizophytoïdes du Crétacé inférieur. Caractéristiques et signification écologique. *Bull. Cent. Rech. Explor.-Prod. Elf-Aquitaine,* 3:685–703.

Masse, J.-P., and Philip, J., 1981. Cretaceous coral-rudist buildups of France. *In* Toomey, D.F. (Ed.), *European Fossil Reef Models.* Spec. Publ.—Soc. Econ. Paleontol. Mineral., 30:399–426.

Milankovitch, M., 1941. Kanon der Erdbestrahlung und seine Anwendung auf das Eiszeitenproblem. *Acad. Royale Serbe, Edition Spec.,* 133.

Minero, C.J., 1991. Sedimentation and diagenesis along open and island-protected windward carbonate platform margins of the Cretaceous El Abra Formation, Mexico. *Sed. Geol.,* 71:261–288.

Monty, C.L.V., 1981. Observations pétrographiques et chimiques sur l'éodiagenèse de carbonates du précontinent calvais (Corse). *Soc. R. Sci. Liège Bull.,* 11-12:470–482.

Monty, C.L.V., Rouchy, J.M., Maurin, A., Bernet-Rollande, M.C., and Perthuisot, J.P., 1987. Reef-stromatolites-evaporites facies relationships from middle Miocene examples of the Gulf of Suez and the Red Sea. *In* Peryt, T.M. (Ed.), *Evaporite Basins.* Lect. Notes Earth Sci., 13:133–188.

Mörner, N.-A., 1994. Internal response to orbital forcing and external cyclic sedimentary sequences. *In* de Boer, P.L., and Smith, D.G. (Eds.), *Orbital Forcing and Cyclic Sequences.* Spec. Publ. Int. Assoc. Sedimentol., 19:25–33.

Müller, D.W., McKenzie, J.A., and Mueller, P.A., 1990. Abu Dhabi sabkha, Persian Gulf, revisited: application of strontium isotopes to test an early dolomitization model. *Geology,* 18:618–621.

Osleger, D., and Read, J.F., 1991. Relation of eustasy to stacking patterns of meter-scale carbonate cycles, Late Cambrian, U.S.A. *J. Sediment. Petrol.,* 61:1225–1252.

Pratt, B.R., and James, N.P., 1986. The St George Group (Lower Ordovician) of western Newfoundland: tidal flat island model for carbonate sedimentation in shallow epeiric seas. *Sedimentology,* 33:313–343.

Read, J.F., and Goldhammer, R.K., 1988. Use of Fischer plots to define third-order sea-level curves in Ordovician peritidal cyclic carbonates, Appalachians. *Geology,* 16:895–899.

Riding, R., 1991. Calcified cyanobacteria. *In* Riding, R. (Ed.), *Calcareous Algae and Stromatolites:* Berlin (Springer-Verlag), 55–87.

Ross, D.J., 1992. Sedimentology and depositional profile of a mid-Cretaceous shelf edge rudist reef complex, Nahal Ha'mearot, northwestern Israel. *Sed. Geol.,* 79:161–172.

Sager, W.W., Winterer, E.L., Firth, J.V., et al., 1993. *Proc. ODP, Init. Repts.,* 143: College Station, TX (Ocean Drilling Program).

Schwarzacher, W., 1993. Cyclostratigraphy and the Milankovitch theory. *Dev. Sedimentol.,* 52.

Scott, R.W., 1988. Evolution of Late Jurassic and Early Cretaceous reef biotas. *Palaios,* 3:184–193.

————, 1990. Models and stratigraphy of Mid-Cretaceous reef communities, Gulf of Mexico. *Soc. Sediment. Geol., Concepts Sedimentol. Paleontol.,* 2.

Shinn, E.A., 1983. Tidal flat environment. *In* Scholle, P.A., Bebout, D.G., and Moore, C. H. (Eds.), *Carbonate Depositional Environments.* AAPG Mem., 33:171–210.

Shinn, E.A., and Lidz, B.H., 1988. Blackened limestone pebbles: fire at subaerial unconformities. *In* James, N.P., and Choquette, P.W. (Eds.), *Paleokarst:* Heidelberg (Springer-Verlag), 117–131.

Strasser, A., 1984. Black-pebble occurrence and genesis in Holocene carbonate sediments (Florida Keys, Bahamas, and Tunisia). *J. Sediment. Petrol.,* 54:1097–1109.

————, 1988. Shallowing-upward sequences in Purbeckian peritidal carbonates (lowermost Cretaceous, Swiss and French Jura Mountains). *Sedimentology,* 35:369–383.

————, 1991. Lagoonal-peritidal sequences in carbonate environments: autocyclic and allocyclic processes. *In* Einsele, G., Ricken, W., and Seilacher, A. (Eds.), *Cycles and Events in Stratigraphy:* Berlin (Springer-Verlag), 709–721.

*Abbreviations for names of organizations and publications in ODP reference lists follow the style given in *Chemical Abstracts Service Source Index* (published by American Chemical Society).

————, 1994. Milankovitch cyclicity and high-resolution sequence stratigraphy in lagoonal-peritidal carbonates (upper Tithonian-lower Berriasian, French Jura Mountains). *In* de Boer, P.L., and Smith, D.G. (Eds.), *Orbital Forcing and Cyclic Sequences.* Spec. Publ.—Int. Assoc. Sedimentol., 19:285–301.

Vail, P.R., 1987. Seismic stratigraphy interpretation using sequence stratigraphy. Part 1: Seismic stratigraphy interpretation procedure. *In* Bally, A.W. (Ed.), *Atlas of Seismic Stratigraphy* (Vol. 1). AAPG Stud. Geol., 27:1–10.

Van Wagoner, J.C., Mitchum, R.M., Campion, K.M., and Rahmanian, V.D., 1990. *Siliciclastic sequence stratigraphy in well logs, cores, and outcrops: concepts for high-resolution correlation of time and facies.* AAPG Methods Explor. Ser., 7.

Winterer, E.L., and Metzler, C.V., 1984. Origin and subsidence of guyots in Mid-Pacific Mountains. *J. Geophys. Res.,* 89:9969–9979.

Wright, V.P., and Tucker, M.E., 1991. Calcretes: an introduction. *In* Wright, V.P., and Tucker, M.E. (Eds.), *Calcretes.* Reprint Ser.—Int. Assoc. Sedimentol., 2:1–22.

Date of initial receipt: 18 November 1993
Date of acceptance: 6 April 1994
Ms 143SR-228

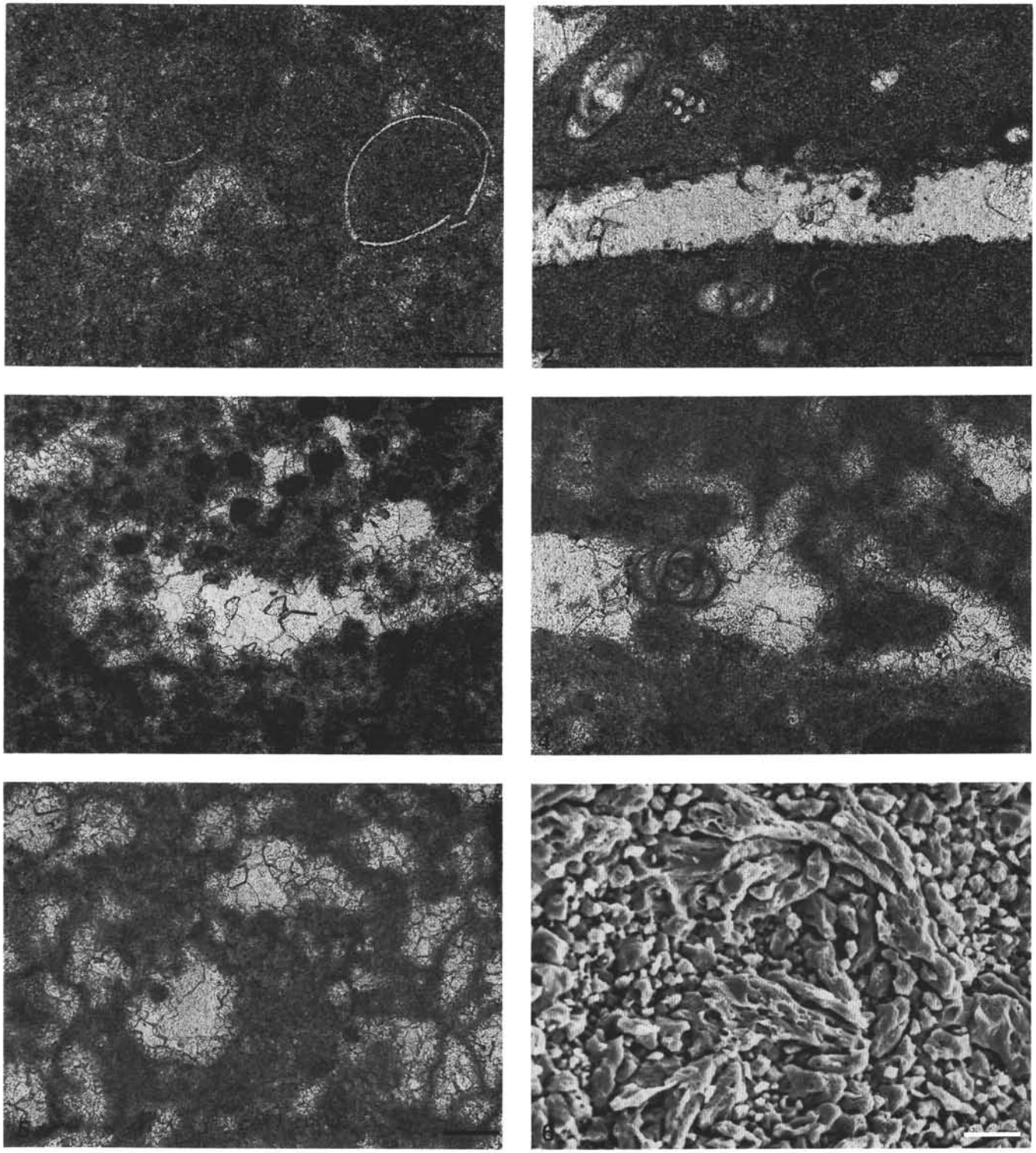

Plate 1. Photomicrographs (nonpolarized light) and SEM micrograph of lagoonal-peritidal facies. **1.** Wackestone with ostracodes (Sample 143-866A-76R-1, 139–143 cm; scale = 0.1 mm). **2.** Wackestone with small benthic foraminifers and bored bivalve shell, now replaced by calcite (Sample 143-866A-146R-1, 111–114 cm; scale 0.1 mm). **3.** Bird's eye in peloidal packstone-grainstone, cemented by calcite (Sample 143-866A-131R-1, 102-105 cm; scale 0.2 mm). **4.** Bird's eye with miliolid foraminifer (same sample as in Fig. 3; scale 0.1 mm). **5.** Thrombolitic algal-microbial structure (Sample 143-866A-46R-1, 85–87 cm; scale = 0.1 mm). **6.** Algal-microbial filaments (same sample as in Fig. 5; scale = 5 μm).

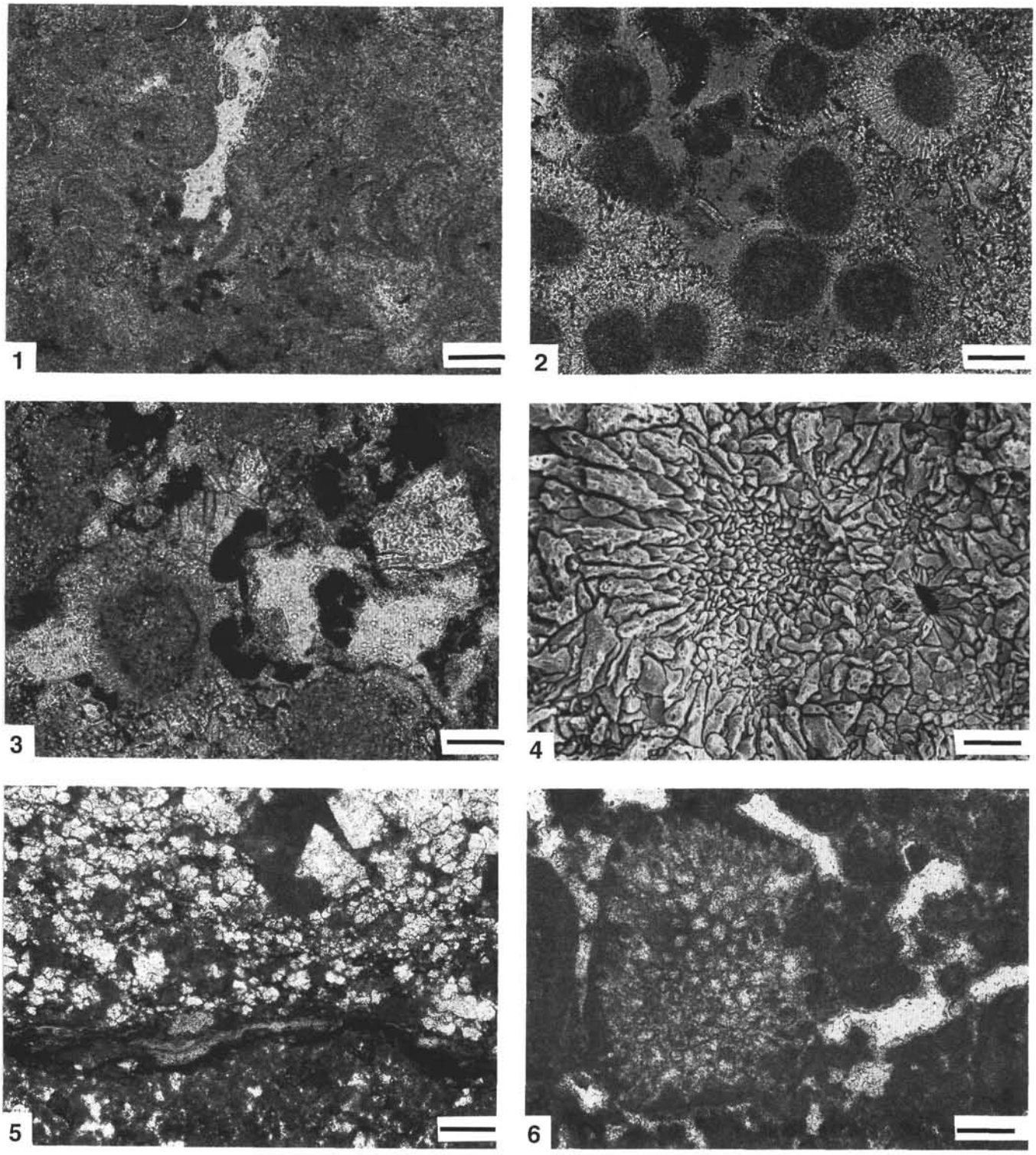

Plate 2. Photomicrographs (nonpolarized light) and SEM micrograph of lagoonal-peritidal facies. **1.** Algal structures resembling *Hormathonema*; dark spots are pyrite (Sample 143-866A-71R-1, 105–107 cm; scale = 0.05 mm). **2.** Spherulites (Sample 143-866A-86R-1, 115–117 cm; scale = 0.05 mm). **3.** Spherulite (lower left), framboidal pyrite (black) and dolomite crystal in upper right corner (Sample 143-866A-130R-1, 57–60 cm; scale = 0.05 mm). **4.** Spherulite displaying fine-grained, structureless center, and rim of elongate crystals; small spherulite to the right with hollow core (same sample as in Fig. 3; scale = 10 µm). **5.** Clay seam apparently confining early dolomitization (Sample 143-866A-128R-1, 53–55 cm; scale = 0.2 mm). **6.** Algal fragment and clotted glaebules bound by micritic meniscus cement and a thin layer of fringing cement (Sample 143-866A-25R-1, 68–70 cm; scale = 0.2 mm).

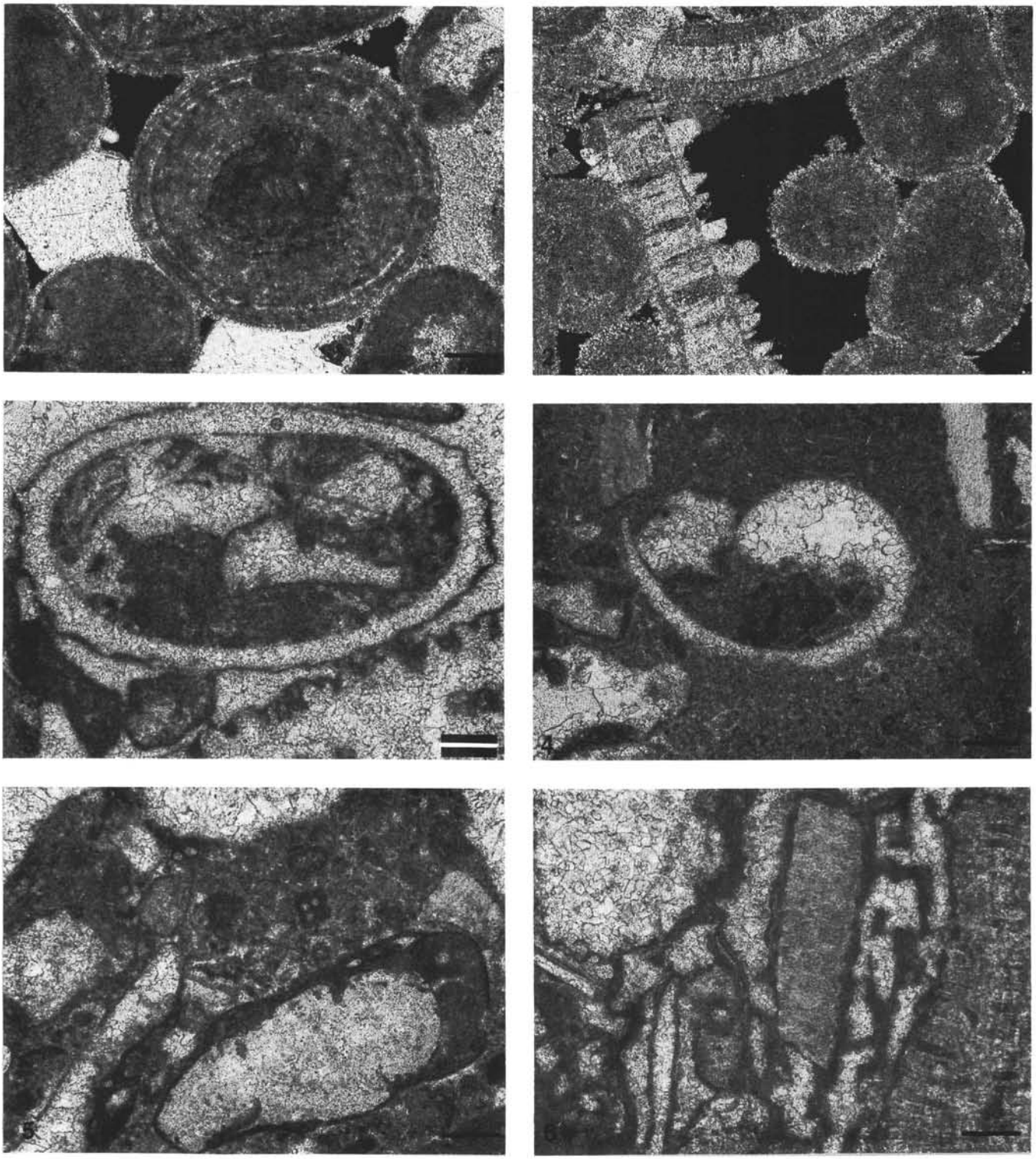

Plate 3. Photomicrographs (1 and 2 polarized, 3 through 6 nonpolarized light) of ooid, storm-beach, and sponge-rudist bioherm facies. **1.** Ooids with radial cortices, cemented by an early fringing and a later blocky cement; porosity shows in black (Sample 143-866A-169R-2, 113–114 cm; scale = 0.1 mm). **2.** Ooid grainstone with bivalve shells, displaying overpacking; porosity is black (Sample 143-866A-154R-1, 110–112 cm; scale = 0.1 mm). **3.** Grainstone to rudstone with dasycladacean algae. Note that only a micrite rind of the original organisms is preserved (Sample 143-867B-1R-3, 15–18 cm; scale = 0.2 mm). **4.** Packstone with dissolved gastropod and algal fragment (lower left). Matrix contains small peloids and thin ostracode fragments (Sample 143-867B-13R-1, 20–22 cm; scale = 0.2 mm). **5.** Bioclasts encrusted by sessile foraminifers. This packstone represents infill between branches of calcareous sponges (Sample 143-868A-2R-2, 74–75 cm; scale = 0.2 mm). **6.** Algal-microbial network between branches of corals and bivalve fragments (Sample 143-868A-4R-1, 62–64 cm; scale = 0.2 mm).